Supplementary File

Nanoengineered Mn_3O_4/rGO Electrophoto-catalyst with Dual Functionality for Detection of 2,4,6-Trichlorophenol and Degradation of Methylene Blue Dye in Environmental Monitoring and Cleanup

Diksha Singh[1], Anshu Kumar Singh[1], Ranjana Verma,[2] Jay Singh[1*]

[1]*Department of Chemistry, Institute of Sciences, Banaras Hindu University, Varanasi (221005), Uttar Pradesh, India*

[2]*Department of Mechanical Engineering, Indian Institute of Technology, Banaras Hindu University (IIT-BHU), Varanasi, (221005), Uttar Pradesh, India*

[*]**Corresponding author** (Email: jaysingh.chem@bhu.ac.in; jaimnnit@gmail.com, ORCID ID: 0000-0002-3793-0450; Phone: +91-9871766453

1. Characterization techniques- The crystallite size of synthesized Mn_3O_4 nanoparticles and Mn_3O_4/rGO NCs has been examined by X-ray diffraction (XRD) using a Rigaku D/Max 2200 diffractometer having Cu Kα radiation source at a wavelength of λ=1.5406 Å. FT-IR spectra of the material have been obtained with a PerkinElmer, Spectrum BX II FTIR spectrophotometer. Raman spectra have been documented in the range of 200-2000 cm^{-1} with the assistance of an argon-ion laser at 514 nm, employing a Renishaw Instruments Raman spectrometer. X-ray photoelectron spectroscopy (XPS) was achieved via an Axis-Nova, Kratos Analytical Ltd., Manchester, UK. Transmission electron microscopy (TEM) was used to determine the average particle size and shape of synthesized Mn_3O_4 nanoparticles and Mn_3O_4/rGO NCs, employing a JEOL JEM-2200 FS (Japan) possesses a tungsten filament at an accelerating voltage of 200 kV, and surface morphology studies of synthesized Mn_3O_4 nanoparticles and Mn_3O_4/rGO NCs via a LEO-440 scanning electron microscope at accelerating voltage of 3 kV. Corrtest CS studio 350 electrochemical workstations are employed to execute electrochemical experiments through CV, DPV, as well as EIS at room temperature (RT). We use a three-electrode arrangement comprising of modified ITO, platinum wire, and Ag/AgCl as working, counter, and reference electrodes in phosphate buffer saline (PBS, 50 mM, pH 7.0, 0.9% NaCl) comprising 5 mM $[Fe(CN)_6]^{3-/4-}$ as a mediator. CV was operated at a scan rate (υ) of 50 mV/s and a potential window from -0.5 V to 0.7 V. The optimized employed parameters for DPV are amplitude (V = 0.05), pulse width (s = 0.1), and pulse period (s = 0.5). The EIS technique operates at the 100,000 to 0.01 Hz frequency range and an amplitude of 5 mV. Most of the electrochemical measurements were executed at room temperature.

2. Results and discussion of GO and rGO-

***(a) XRD study*:** GO is considered by the sharp peak at the angle 2θ at 11.02º corresponding to the (001) plane, and for rGO, it has a characteristic broad peak at nearly 2θ at 25.8º corresponding to the (002) plane, as it is represented in Figure S1(a).

***(b) Raman study*:** Two bands, G and D, appear in the Raman spectra of GO and rGO. The G band is located around 1583 cm^{-1}, and the D band is around 1360 cm^{-1} in GO *(1)*. The G band results from sp^2 carbon vibration in the graphitic carbon. The D band originates due to the disordered vibration in carbon atoms and structural defects on the surface of the nanomaterial *(1,2)*. In rGO, the D peak shifts to 1348 cm^{-1}, and the G band at around 1578 cm^{-1} *(3)*. For GO, the I_D/I_G ratio is 0.93, and for rGO, it is 0.96 as it is represented in Figure S1(b).

***(c) FTIR study*:** GO exhibits strong absorption FTIR bands at 3430 cm^{-1} corresponding to the O-H component of the adsorbed water molecules and carboxylic acid, 1630 cm^{-1} attributed to the carbonyl group, 1055 cm^{-1} and 585 cm^{-1} attributed to the stretching and bending band of the C-O-C bond of the epoxy group. For rGO, 3436 cm^{-1} corresponds to the O-H component of the adsorbed water molecules. From FTIR spectra, we found that most of the functional groups are diminished or reduced in rGO as compared to GO, which validates the successful reduction of GO into rGO as it is represented in Figure S1(c) which was further validates from the EDAX mapping where it was confirms from the weight% and atomic% matrix of the GO and rGO where rGO having less oxygen content than GO.

.

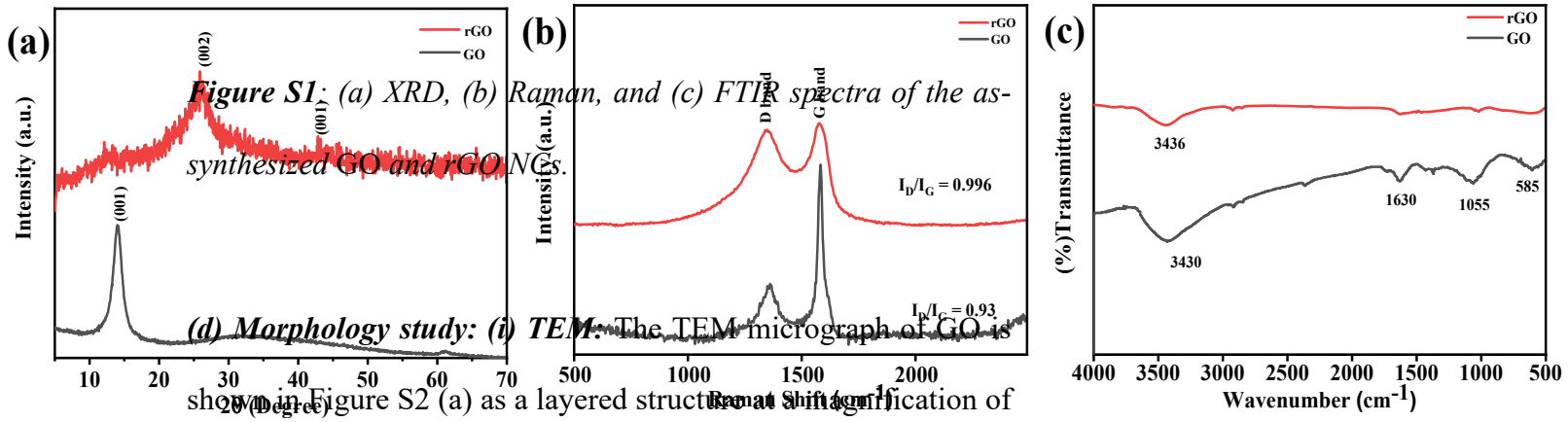

Figure S1*: (a) XRD, (b) Raman, and (c) FTIR spectra of the as-synthesized GO and rGO NCs.*

(d) Morphology study: (i) TEM: The TEM micrograph of GO is shown in Figure S2 (a) as a layered structure at a magnification of 100 nm scale. Similarly, the TEM of rGO is shown in Figure S2 (d) as a layered structure at a magnification of 50 nm.

(ii) SEM and EDAX: SEM of the GO shown in Figure S2 (b) as a folded layered structure at a magnification of 200 nm. Similarly, the SEM of rGO is shown in Figure S2 (e) as a layered structure at a magnification of 200 nm. From the SEM image of GO, it has more folds than rGO. The curved rGO surface specifies the elimination of the oxygen-bearing functional group, which is further validated by the EDAX image of the GO and rGO shown in Figures S2 (c) and S2 (f), as element weight% and atomic% signify that there is less oxygen-containing functional group in rGO than in GO.As we know that there are various oxygen-bearing functional groups (OFs) like epoxy, carbonyl, hydroxyl, and carboxyl groups *(4)*, and these are non-conducting nature of GO is due to the hindrance created in conjugation via the OFs. rGO is chemically and thermally reduced from GO, having fewer OFs and increased electrical conductivity.

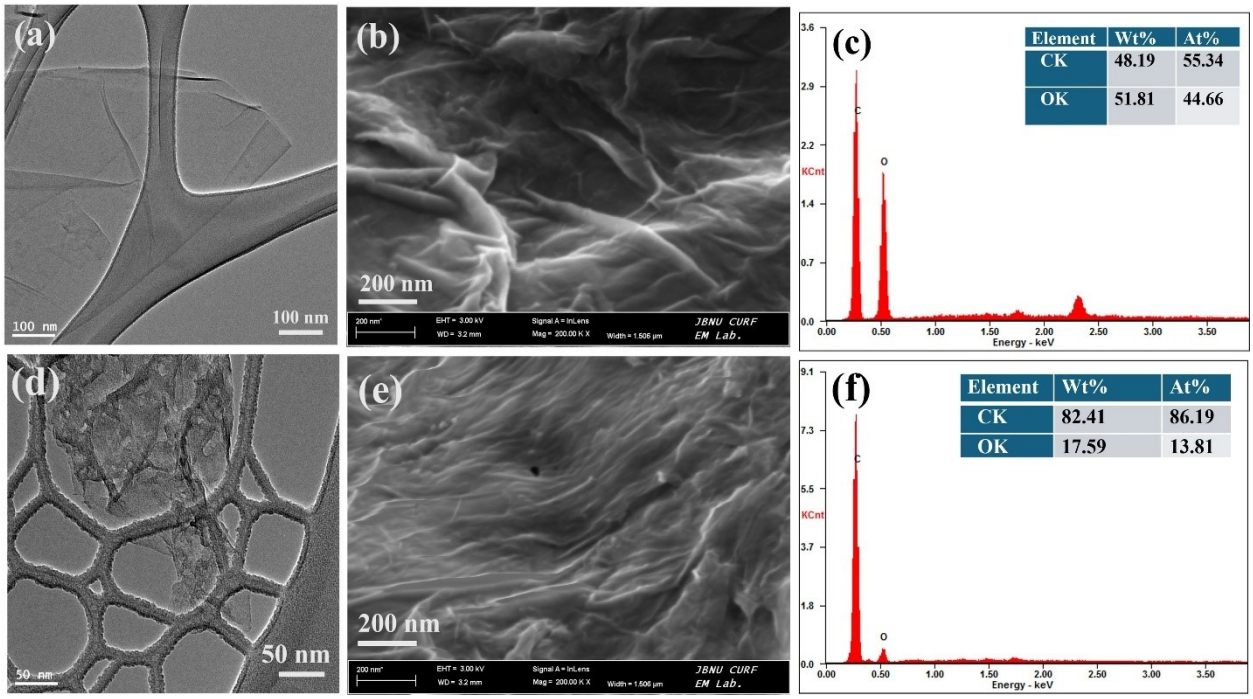

Figure S2*: (a) The TEM portrait of the GO, (b) The SEM portrait of GO NMs, (c) EDS energy spectrum of GO NMs, (d) The TEM portrait of the rGO, (e) The SEM portrait of rGO NMs, (f) EDS energy spectrum of rGO NMs.*

3. Photocatalytic Degradation experiments- The photocatalytic action of individual samples was examined under UV and Visible light to demonstrate the degradation of methylene blue (MB). Here, we prepared a 20 ppm solution of MB dye, and 30 mg of the catalyst was mixed into 30 mL of this dye solution and kept in the dark for 1 hr to attain adsorption-desorption equilibrium for Mn_3O_4 and Mn_3O_4/rGO, respectively. The catalyst-loaded MB solution is kept under UV and Visible light separately, and sampling is carried out at every 10-minute intervals. The catalyst Mn_3O_4/rGO degrades MB in irradiation of the UV light, and the catalyst Mn_3O_4 shows minute degradation. Both catalysts show very minute degradation in irradiation of Visible light. So, we performed degradation in UV light, during the given time interval, the solution is centrifuged and

examined by recording the peculiarity of the absorption determined at 664 nm utilizing a Shimadzu 1900, UV-visible spectrophotometer.

3.1. Photodegradation of MB dye with rGO: For this experiment, a 20 ppm solution of the dye was prepared. Then, 30 mg of the rGO was mixed into 30 mL of this dye solution. This solution was mixed continuously in the dark for 60 minutes to allow the MB dye and the rGO to reach a stable adsorption-desorption state. After this initial phase, the solution was exposed to UV light to monitor how effectively the dye was broken down in the proximity of the rGO. Throughout the experiment, a rGO solution with MB of approximately 3 mL was taken from the dye solution after every 10 minutes using a micropipette to track the progress of the degradation process. The magnitude of the absorption peak at 664 nm, characteristic of MB, was observed to decrease. A substantial drop in this absorption intensity was observed within 80 minutes when using the rGO catalyst. The MB dye degradation reached up to 50% with the rGO catalyst when exposed to UV light for 80 minutes, as presented in Figure S3. Figure S4 represents absorption spectra of the scavenging analysis in the presence and absence of different scavengers.

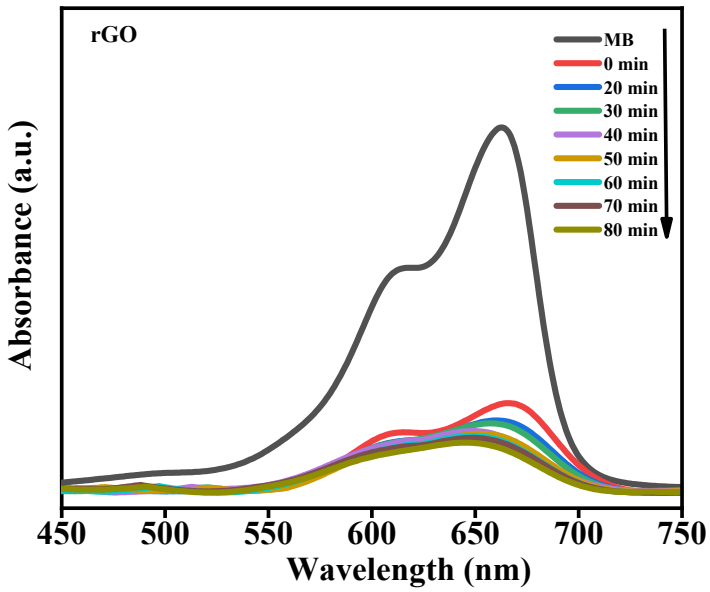

Figure S3: Absorption spectra showing the breakdown of MB in the presence of rGO

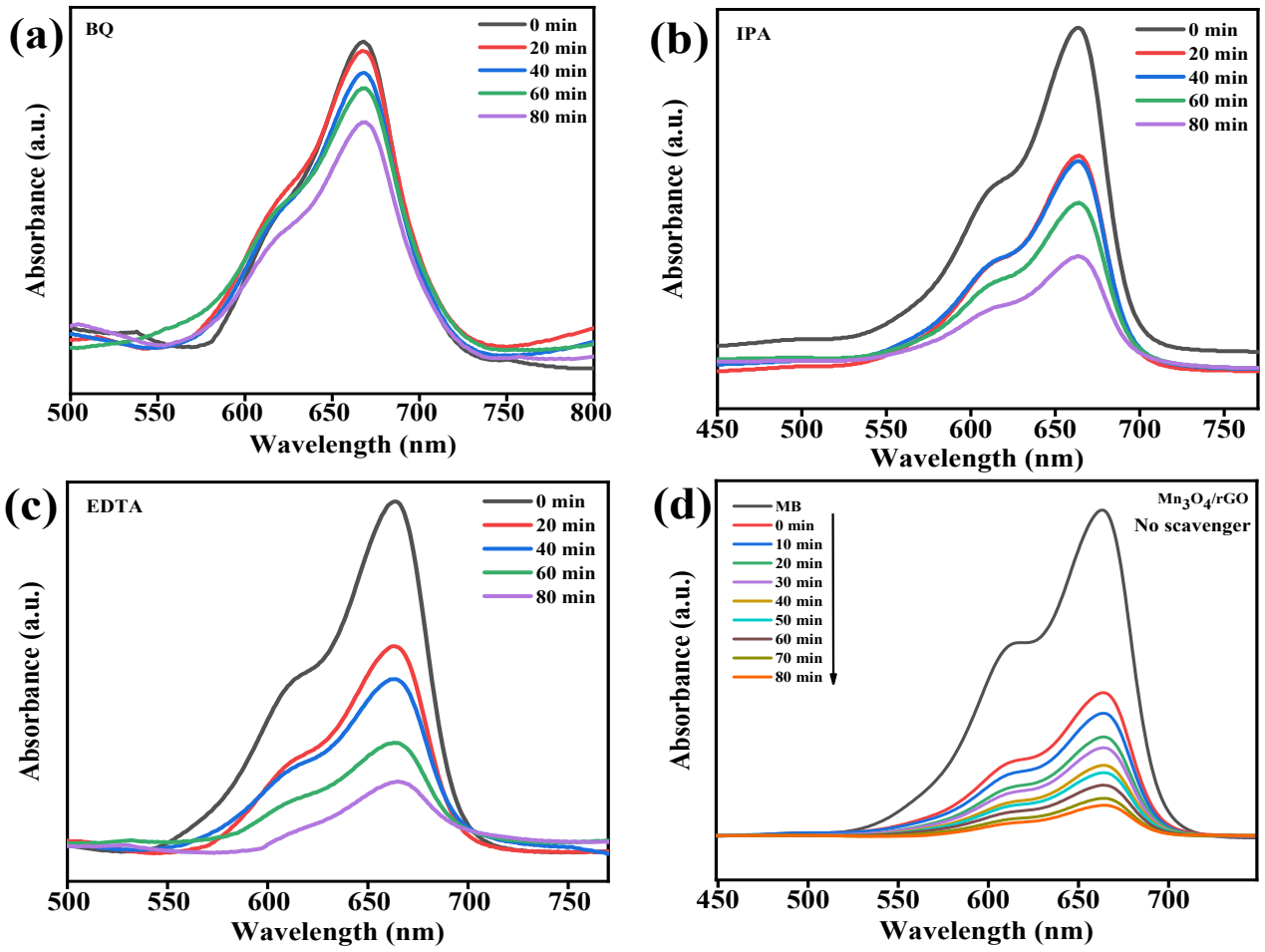

Figure S4 Photodegradation of methylene blue (MB) dye using Mn3O4/rGO NCs with (a) p-benzoquinone (pBQ)- superoxide radical scavenger (b) IPA hydroxyl radical scavenger (c) EDTA hole scavenger (d) No scavenger

Table S1- Scan rate analysis of Mn_3O_4/rGO/ITO electrode during 2,4,6-TCP sensing

S. No.	**Scan Rate (mV/s)**	**Square root of Scan Rate**	**E_{pa} (V)**	**E_{pc} (V)**	**E= (E_{pa}-E_{pc}) in mV**
1.	10	3.1622776602	0.348335613	0.176607387	171.728226
2.	20	4.472135955	0.368445052	0.158093935	210.351117
3.	30	5.4772255751	0.383128135	0.149156407	233.971728
4.	40	6.3245553203	0.392065663	0.142134063	249.9316
5.	50	7.0710678119	0.403237574	0.129685363	273.552211
6.	60	7.7459666924	0.412813497	0.125535796	287.277701
7.	70	8.366602653	0.416005472	0.123620611	292.384861
8.	80	8.94427191	0.423027816	0.110852713	312.175103
9.	90	9.4868329805	0.429411765	0.112129503	317.282262
10.	100	10	0.429730962	0.104149567	325.581395

Table S2- Response time analysis of Mn_3O_4/rGO/ITO electrode

S. No.	Response time (Second)	Current (mA)	Recovery percent (%)	RSD (%)
1.	0	0.928720996	100	0
2.	5	0.946179966	101.88	1.88
3.	10	0.946179966	101.88	1.88
4.	15	0.944142615	101.66	1.66
5.	20	0.944142615	101.66	1.66
6.	25	0.94516129	101.77	1.77
7.	30	0.939388795	101.15	1.15
8.	35	0.936332767	100.82	0.82
9.	40	0.935314092	100.71	0.71

10.	45	0.933616299	100.53	0.53
11.	50	0.929881154	100.13	0.13
12.	55	0.893237125	96.18	3.82
13.	60	0.891680815	96.01	3.99
14.	65	0.875183928	94.24	5.76

Table S3- Stability analysis of Mn_3O_4/rGO/ITO electrode

S. No.	**Number of days**	**Current (mA)**	**Recovery percent (%)**	**RSD (%)**
1.	1	0.896774194	100	0
2.	2	0.897849462	100.12	0.12
3.	3	0.896236559	99.94	0.06
4.	4	0.899462366	100.29	0.29
5.	5	0.903225806	100.72	0.72
6.	10	0.901075269	100.48	0.48

7.	15	0.901612903	100.54	0.54
8.	20	0.9	100.36	0.36
9.	25	0.895698925	99.88	0.12
10.	30	0.898924731	100.24	0.24
11.	35	0.899462366	100.29	0.29
12.	40	0.897849462	100.12	0.12
13.	45	0.896774194	100.00	0.00
14.	50	0.897849462	100.12	0.12
15.	55	0.896236559	99.94	0.06
16.	60	0.895698925	99.88	0.12

Table S4- Reusability analysis of Mn_3O_4/rGO/ITO electrode

S. No.	**Number of Scans**	**Current (mA)**	**Recovery percent (%)**	**RSD (%)**
1.	1 Scan	0.682314658	100	0
2.	2 Scan	0.682767402	100.07	0.07
3.	3 Scan	0.684804754	100.37	0.37
4.	4 Scan	0.686162988	100.55	0.55
5.	5 Scan	0.686842105	100.66	0.66
6.	6 Scan	0.685936616	100.53	0.53

7.	7 Scan	0.683899264	100.23	0.23
8.	8 Scan	0.685710243	100.49	0.49
9.	9 Scan	0.67416525	98.81	1.19
10.	10 Scan	0.666242218	97.65	2.35
11.	11 Scan	0.648005093	94.97	5.03
12.	12 Scan	0.649702886	95.22	4.78
13.	13 Scan	0.644821732	94.51	5.49
14.	14 Scan	0.643972835	94.38	5.62
15.	15 Scan	0.626358234	91.79	8.21
16.	16 Scan	0.566808149	83.07	16.93

Table S5- Interference analysis of the 2,4,6-TCP on the Mn_3O_4/rGO/ITO electrode

S. No.	**Interferent with standard (50µM)**	**Current (mA)**	**Recovery percent (%)**	**RSD (%)**
1.	2,4,6-Trichlorophenol [2,4,6-TCP]	0.840067912	100	
2.	2 Bromophenol+ 2,4,6-TCP	0.875721562	104.25	4.25
3.	4 Bromophenol+ 2,4,6-TCP	0.866044143	103.09	3.09
4.	2,4-Dibromophenol+ 2,4,6-TCP	0.834465195	99.33	0.664

5.	2-Chlorophenol+ 2,4,6-TCP	0.872156197	103.82	3.82
6.	4-Chlorophenol+ 2,4,6-TCP	0.86196944	102.61	2.61
7.	2,4-Dichlorophenol+ 2,4,6-TCP	0.841595925	100.18	0.18
8.	2-Nitrophenol+ 2,4,6-TCP	0.848726655	101.03	1.03
9.	4-Nitrophenol+ 2,4,6-TCP	0.829371817	98.73	1.27
10.	2,4-Dinitrophenol+ 2,4,6-TCP	0.841595925	100.18	0.18

Table S6- Real Sample analysis of the 2,4,6-TCP on the Mn_3O_4/rGO/ITO electrode

S. No.	**Real sample with standard (60µM)**	**Current (mA)**	**Determination of concentration in real sample (µM)**	**Recovery percent (%)**	**RSD (%)**
1.	2,4,6 -TCP (60 µM)	0.823259762	60	100	0
2.	2,4,6 -TCP (60 µM) +BW	0.855857385	62.38	103.96	3.96
3.	2,4,6 -TCP (60	0.834465195	60.82	101.36	1.36

	µM) +DW				
4.	2,4,6 -TCP (60 µM) +GRW	0.870628183	63.45	105.75	5.75
5.	2,4,6-TCP (60 µM) +TW	0.860441426	62.71	104.52	4.52

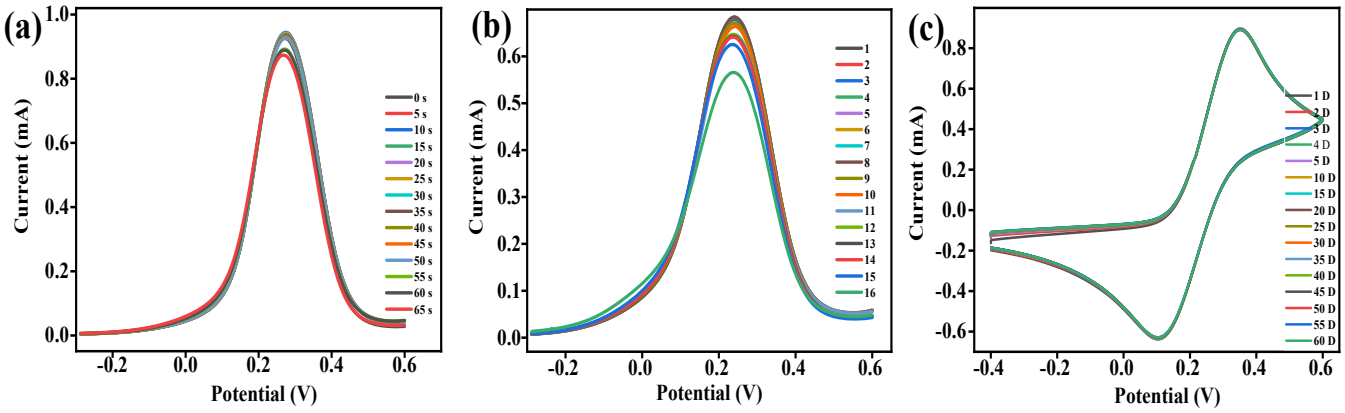

Figure S5: *(a) CV Curve of Response time (b) Reusability and (c) Stability analysis of the prepared Mn_3O_4/rGO/ITO electrode*

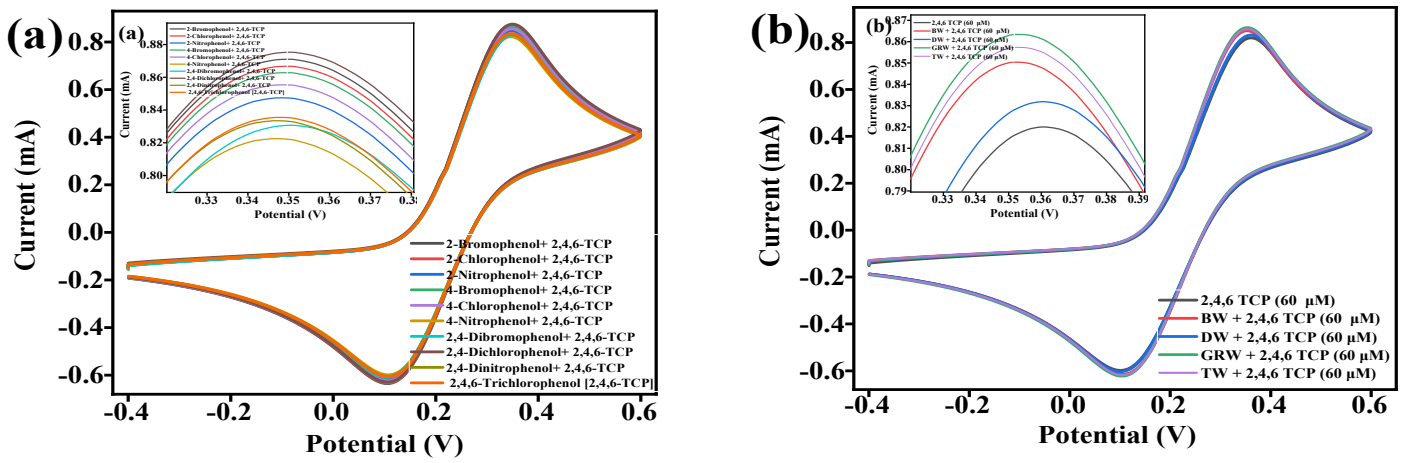

Figure S6: *(a) CV Curve of Interference study of 2,4,6-TCP and (b) Real sample analysis of 2,4,6-TCP on Mn_3O_4/rGO/ITO electrode.*

Figure S7: Tem Image Mn_3O_4

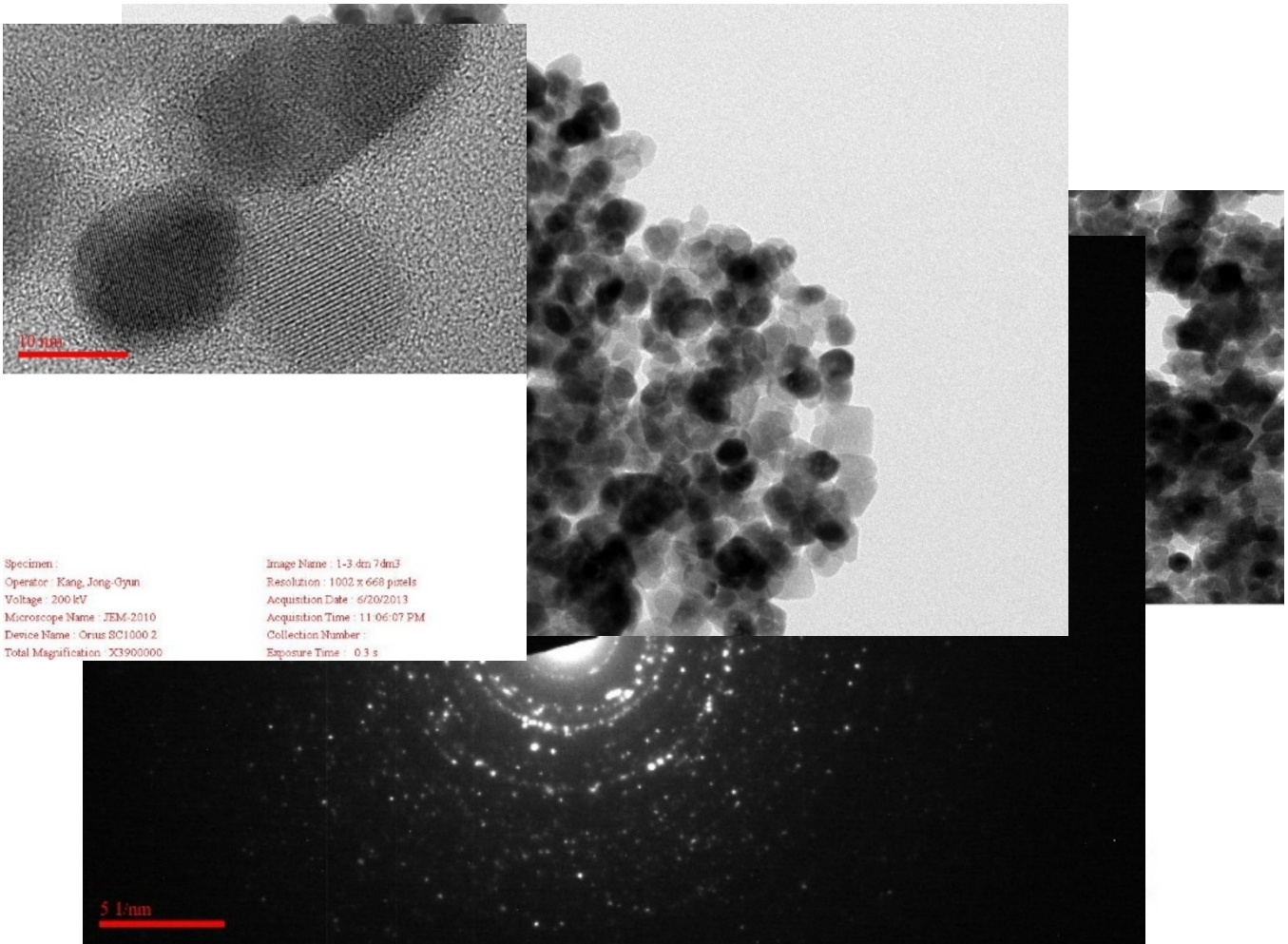

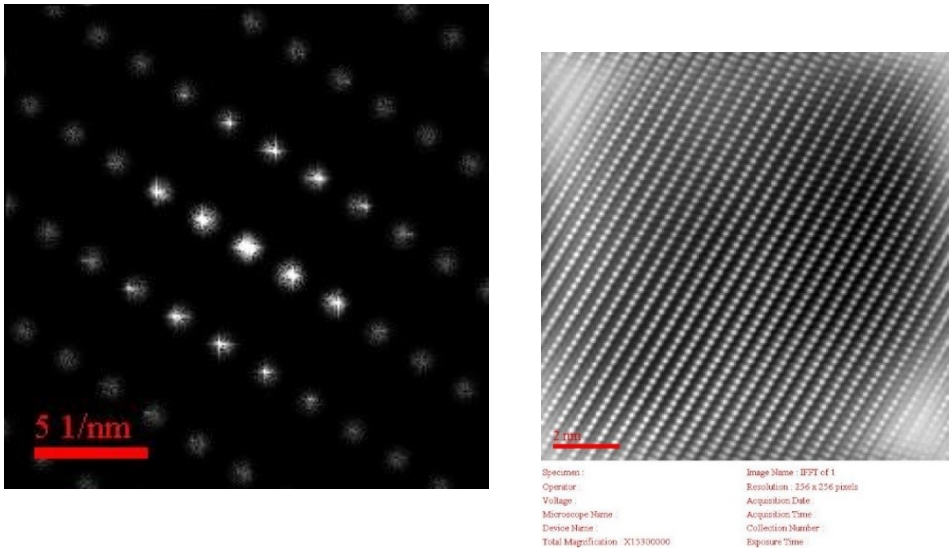

Figure S8: Tem Image Mn_3O_4/rGO

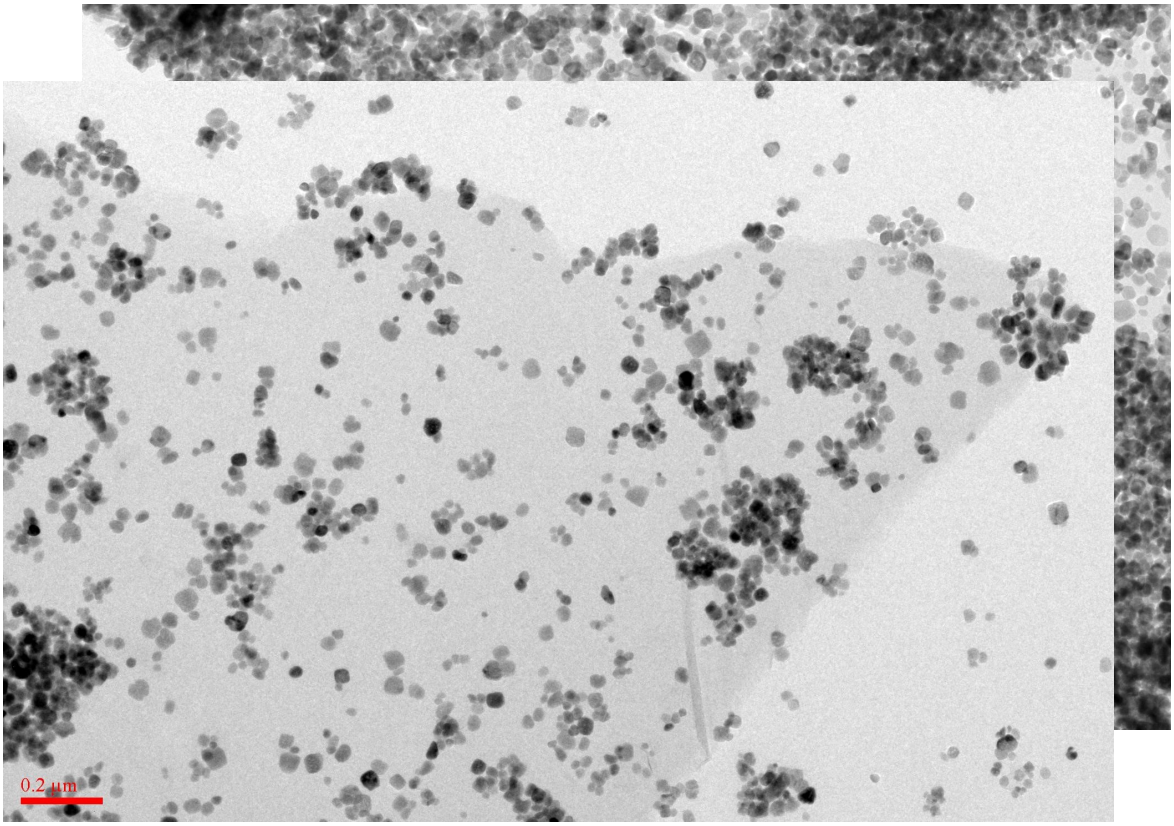
0.2 µm

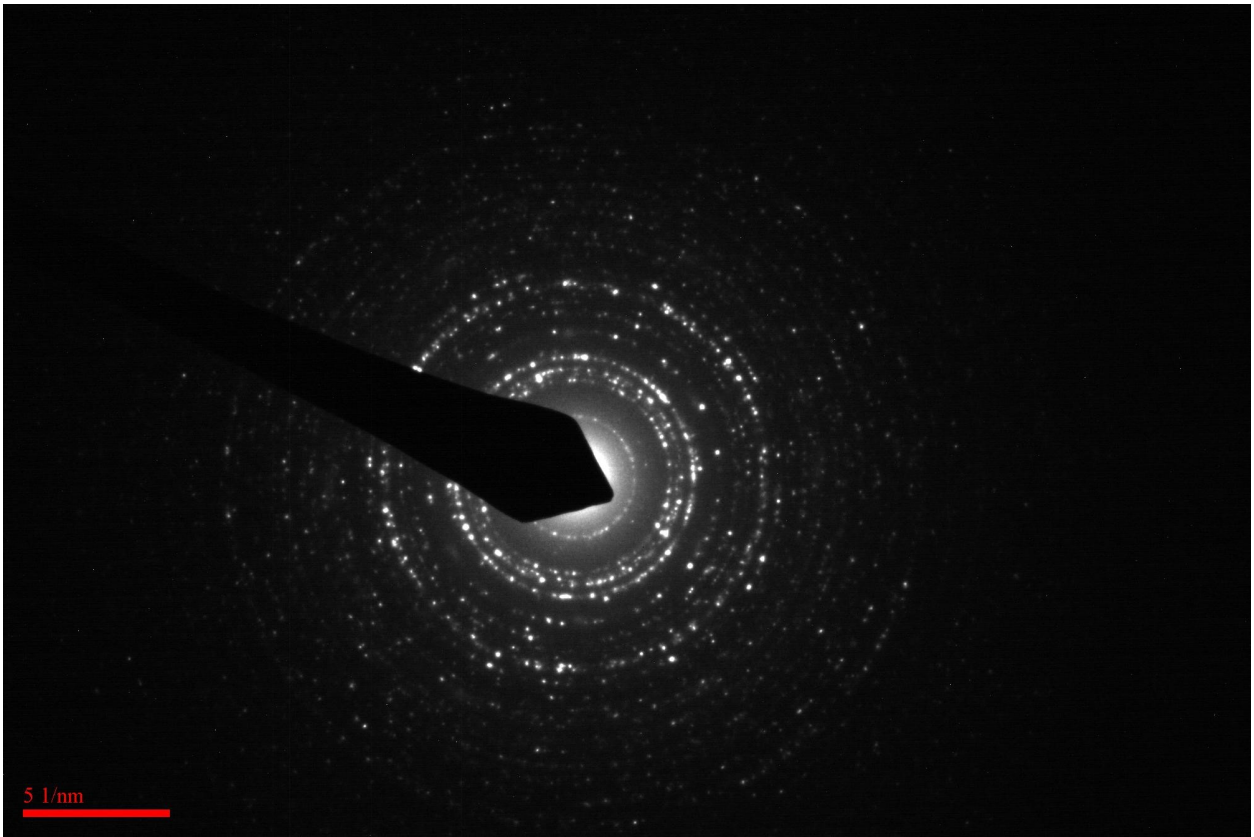
5 1/nm

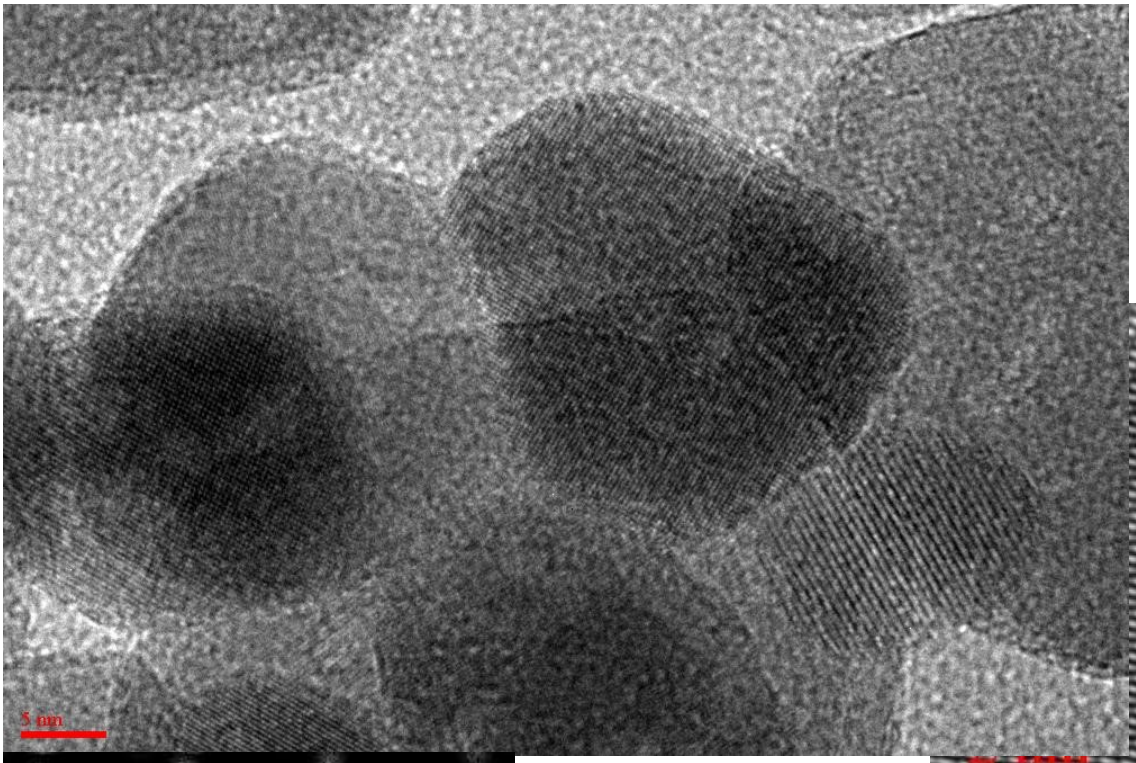
5 nm

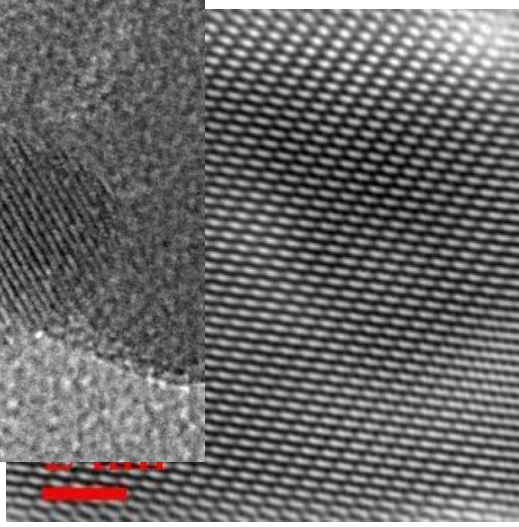

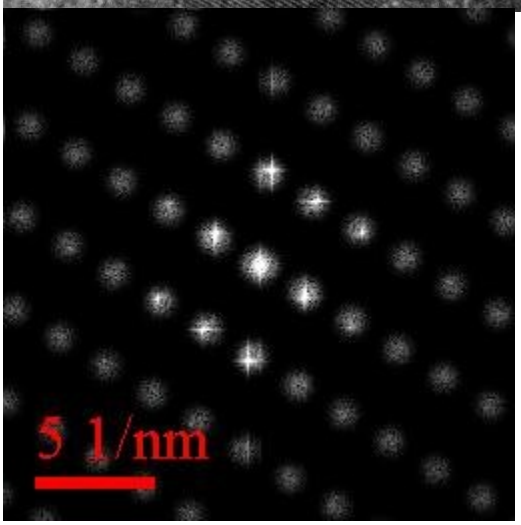
5 1/nm

Figure S9: Sem Image of Mn_3O_4

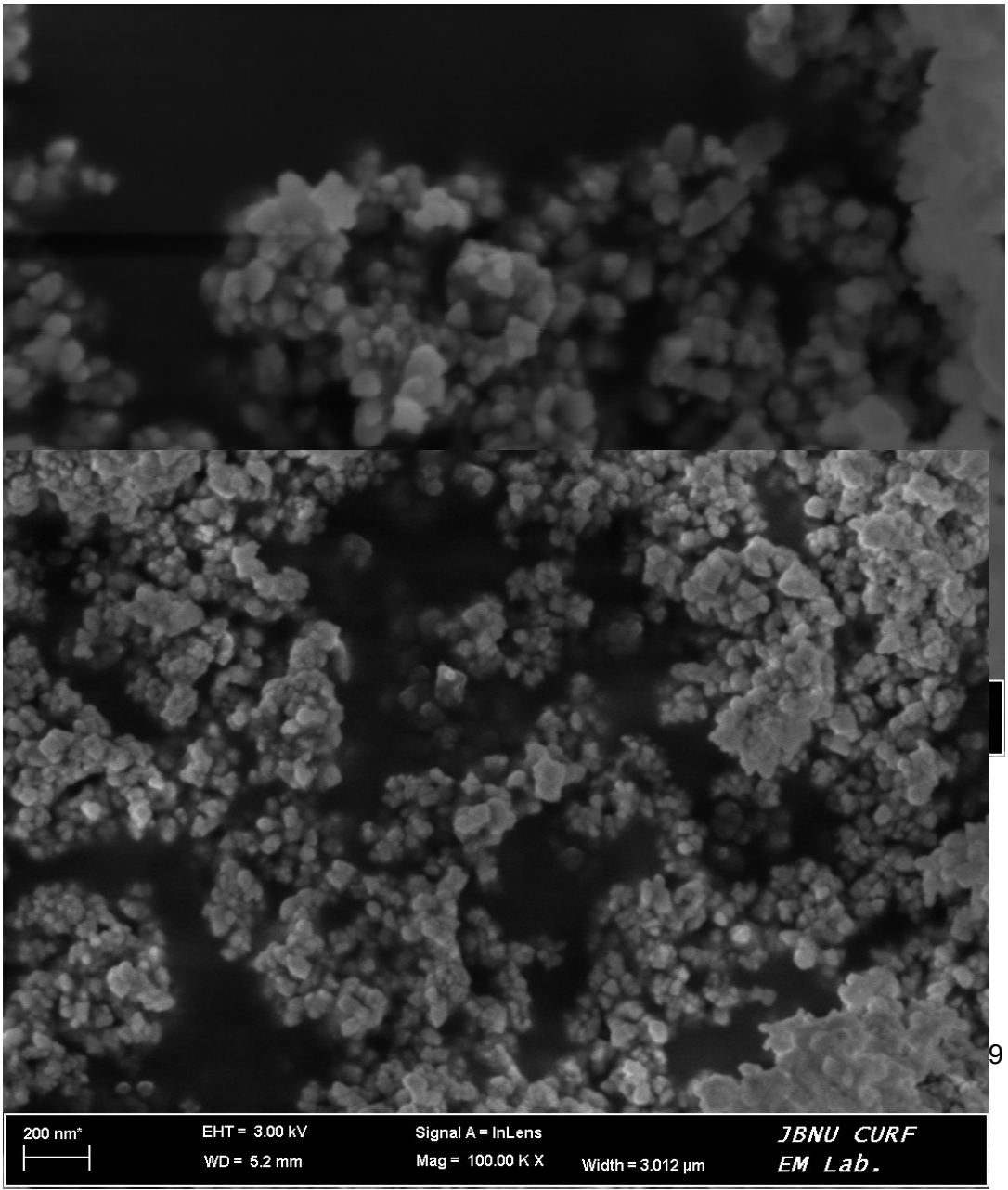

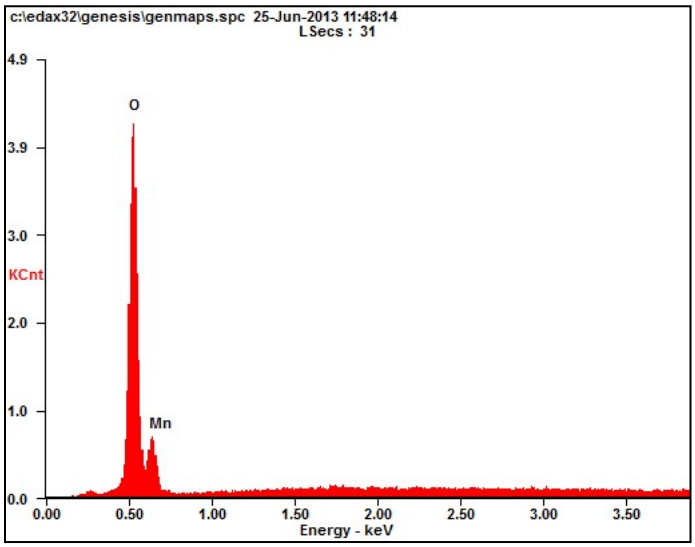

Element	*Wt%*	*At%*
OK	26.60	55.44
MnK	73.40	44.56
Matrix	Correction	ZAF

EDAX mapping of Mn_3O_4

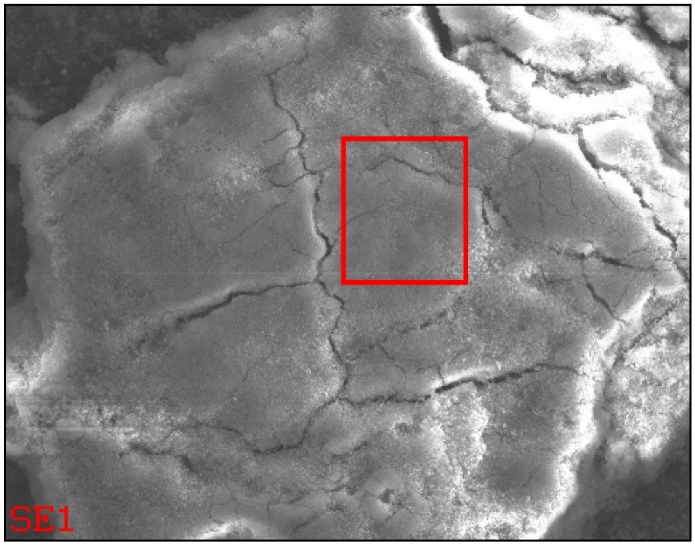

Figure S10: Sem Image of Mn_3O_4/rGO

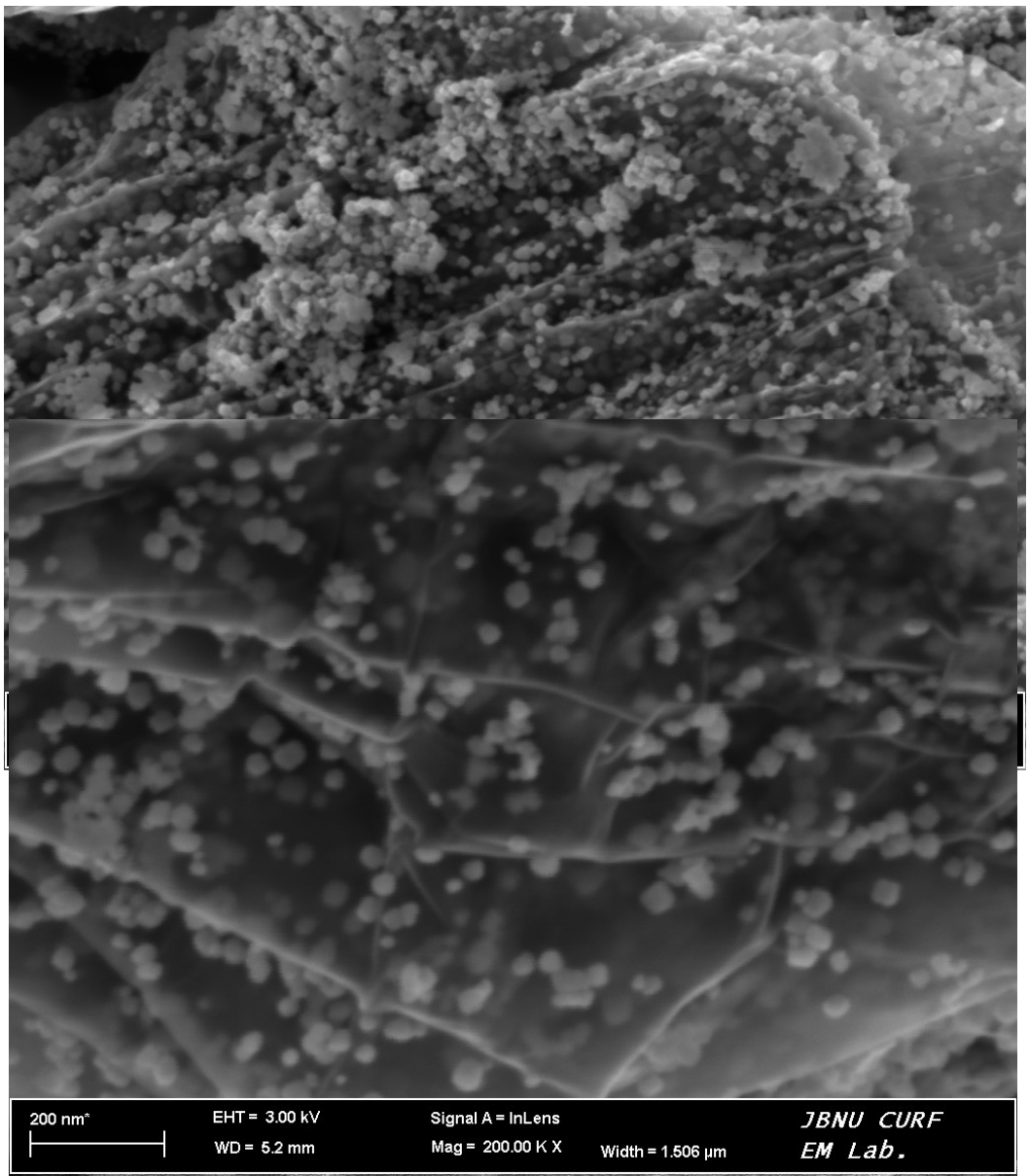

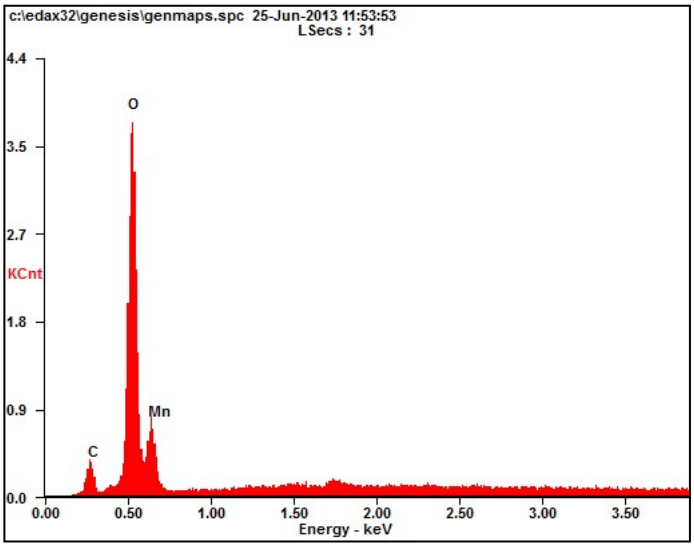

Edax mapping of Mn_3O_4/rGO

Element	*Wt%*	*At%*
CK	05.91	14.54
OK	26.58	49.12
MnK	67.52	36.34
Matrix	Correction	ZAF

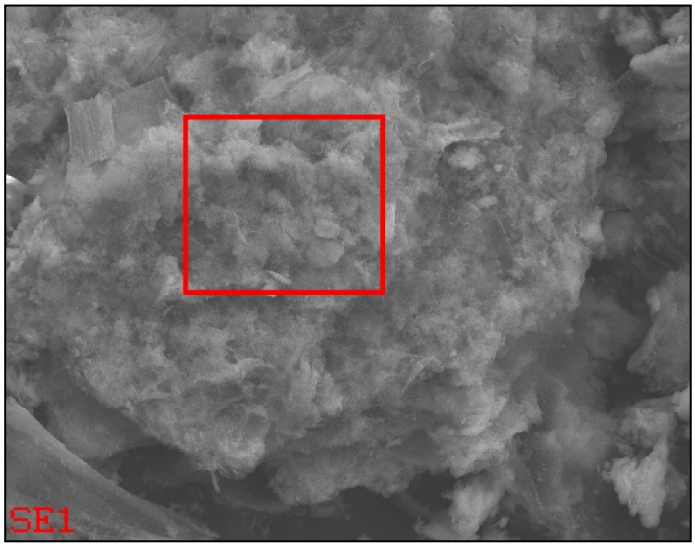

Figure S11: TEM Image GO

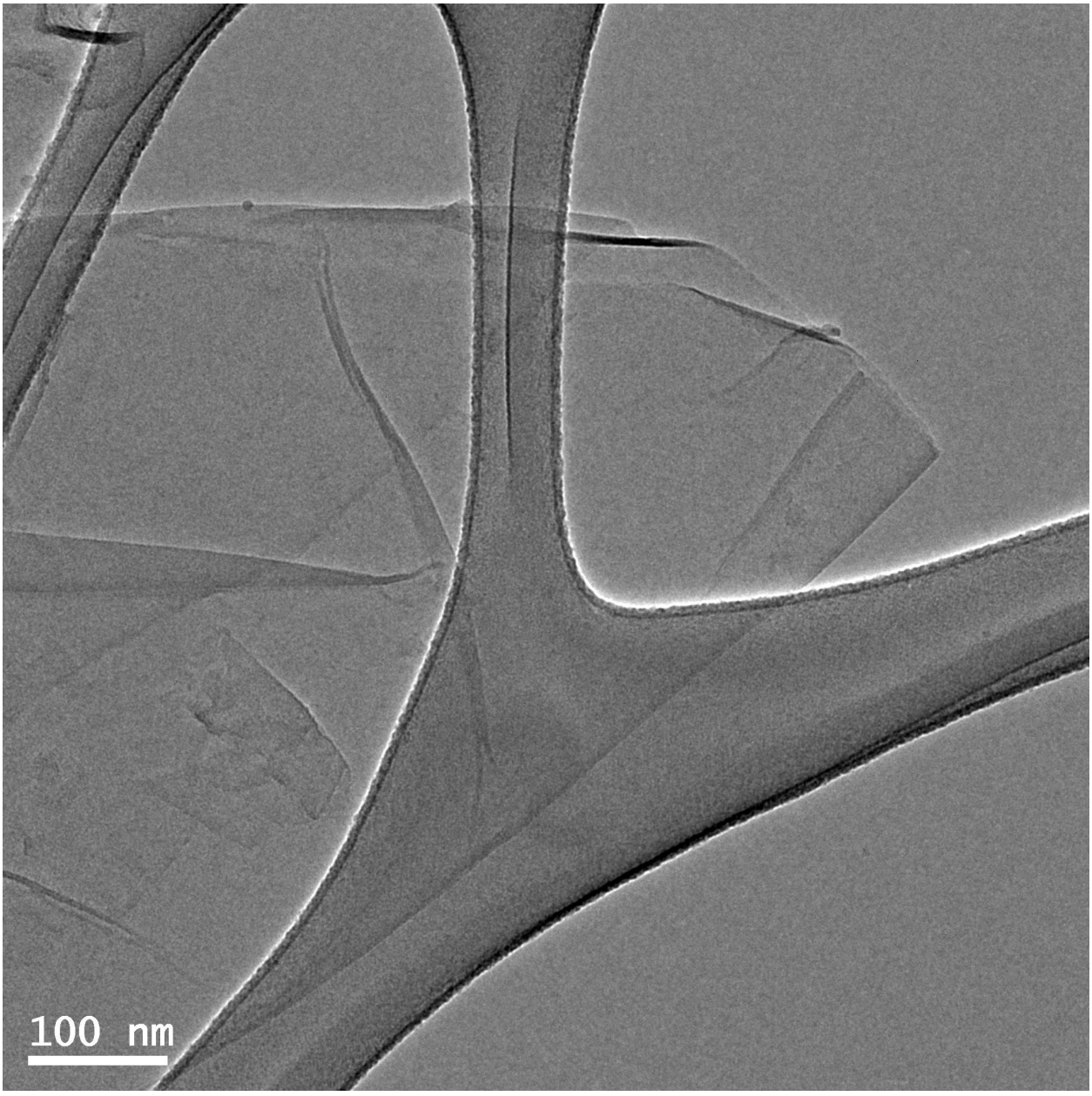

Figure S12: TEM Image rGO

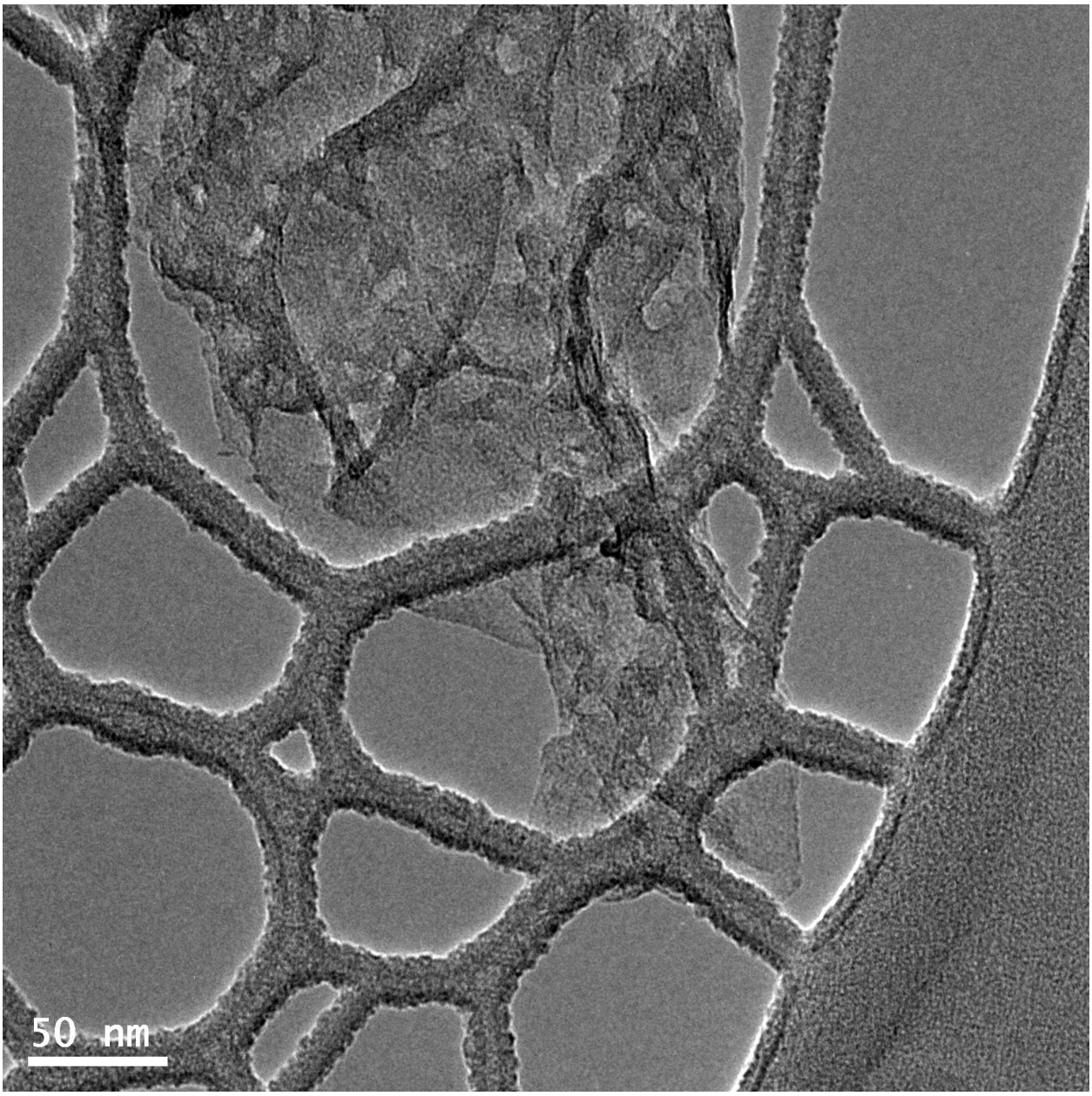

Figure S13: SEM Image of GO

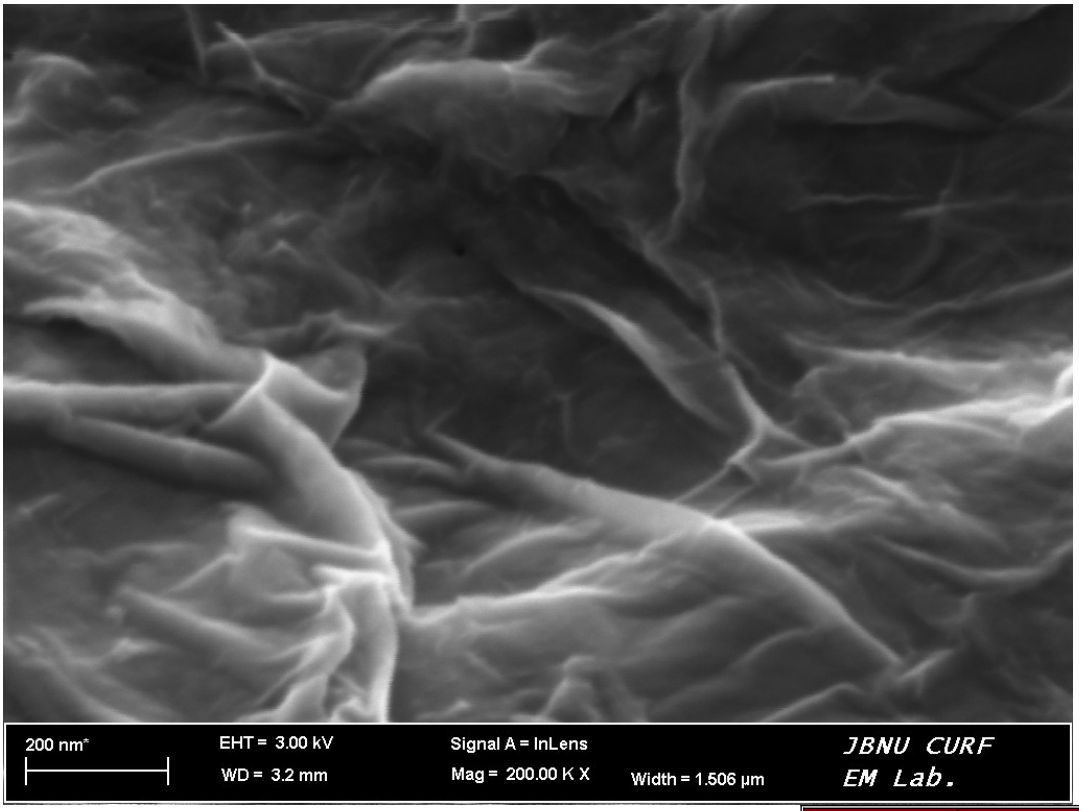

Element	*Wt%*	*At%*
CK	48.19	55.34

EDAX mapping of GO

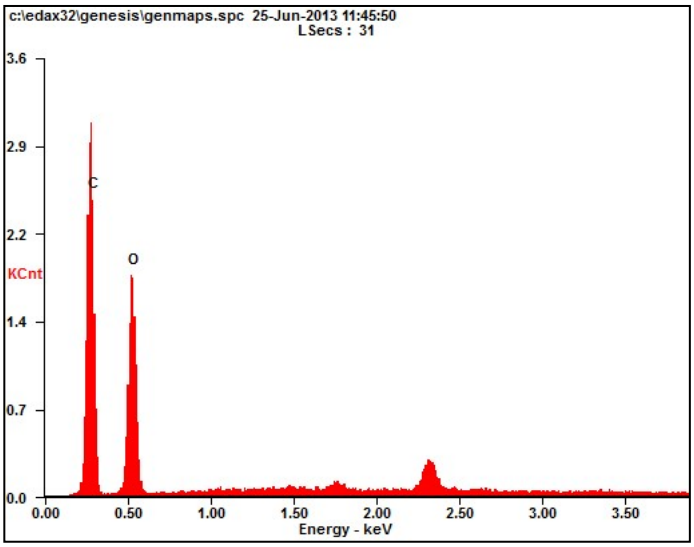

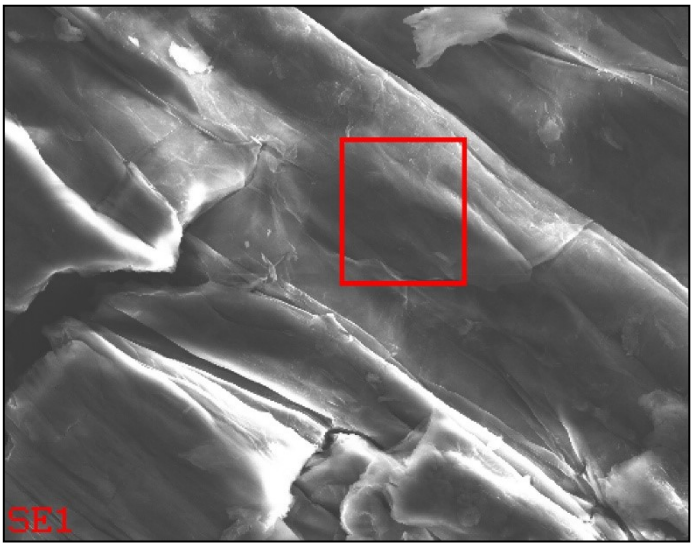

OK	51.81	44.66
Matrix	Correction	ZAF

Figure S14: SEM Image of rGO

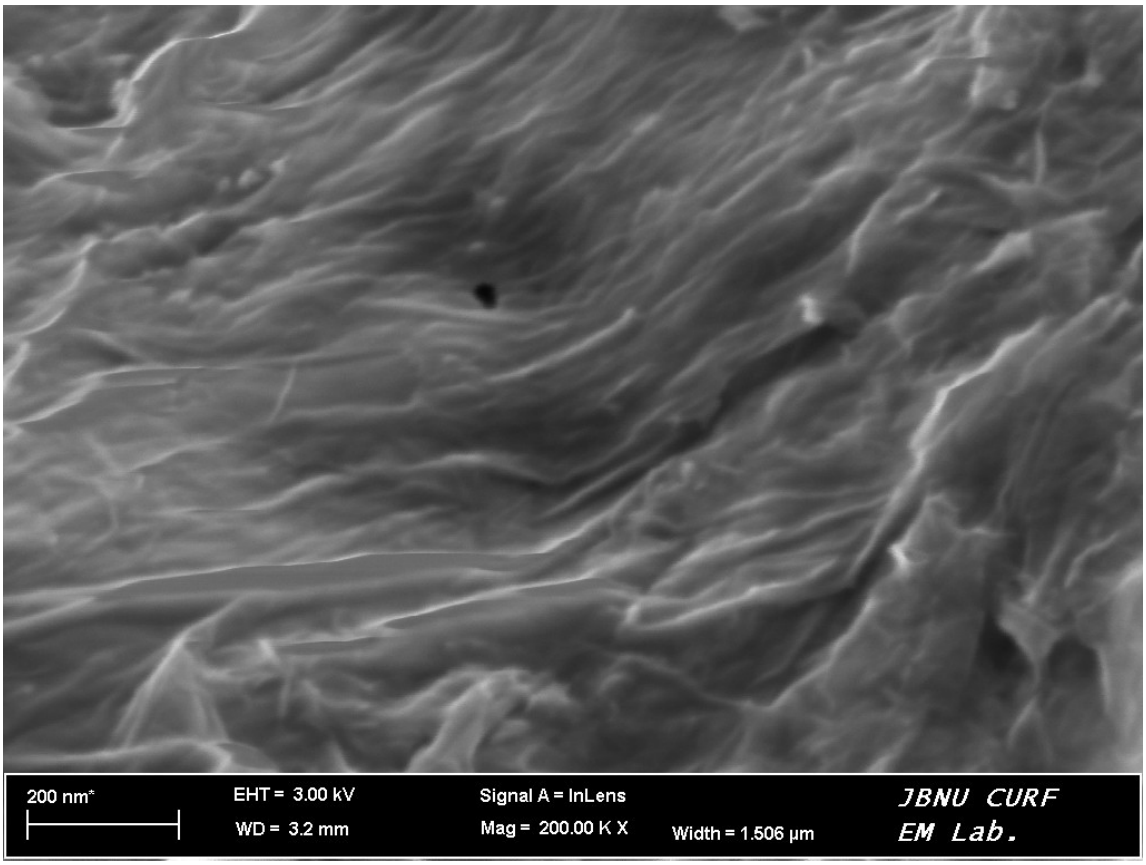

EDAX mapping of rGO

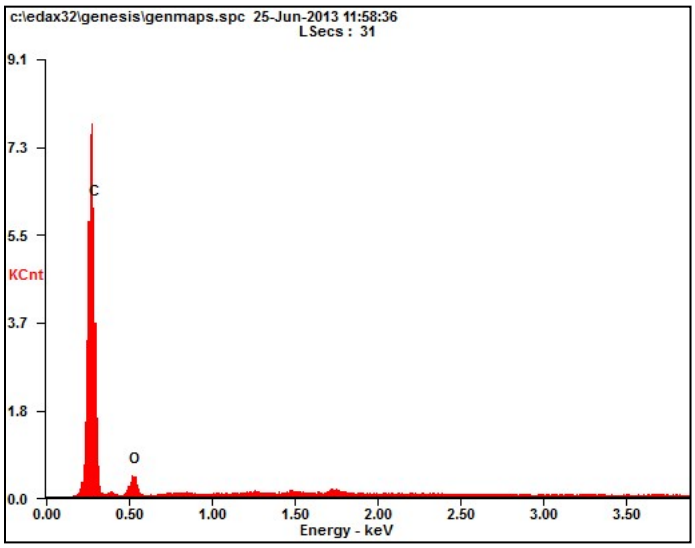

Element	*Wt%*	*At%*
CK	82.41	86.19
OK	17.59	13.81
Matrix	Correction	ZAF

References-

1. Yang, K.; Huang, X.; Fang, L.; He, J.; Jiang, P. Fluoro-polymer functionalized graphene for flexible ferroelectric polymer-based high-k nanocomposites with suppressed dielectric loss and low percolation threshold. *Nanoscale* **2014**, *6*(24), 14740–14753. doi:10.1039/C4NR03957B.

2. Díez, N.; Śliwak, A.; Gryglewicz, S.; Grzyb, B.; Gryglewicz, G. Enhanced reduction of graphene oxide by high-pressure hydrothermal treatment. *RSC Advances* **2015**, *5*(100), 81831–81837. doi:10.1039/C5RA14461B.

3. Huang, H.-H.; De Silva, K. K. H.; Kumara, G. R. A.; Yoshimura, M. Structural Evolution of Hydrothermally Derived Reduced Graphene Oxide. *Scientific Reports* **2018**, *8*(1), 6849. doi:10.1038/s41598-018-25194-1.

4. Chee, W. K.; Lim, H. N.; Zainal, Z.; Huang, N. M.; Harrison, I.; Andou, Y. Flexible Graphene-Based Supercapacitors: A Review. *The Journal of Physical Chemistry C* **2016**, *120*(8), 4153–4172. doi:10.1021/acs.jpcc.5b10187.